The Astrophysical Journal Supplement Series, 247:59 (8pp), 2020 April https://doi.org/10.3847/1538-4365/ab765f

Submillimeter and Far-infrared Spectroscopy of Monodeuterated Amidogen Radical (NHD): Improved Rest Frequencies for Astrophysical Observations

Luca Bizzocchi[1], Mattia Melosso[2], Barbara Michela Giuliano[1], Luca Dore[2], Filippo Tamassia[3], Marie-Aline Martin-Drumel[4], Olivier Pirali[4,5], Laurent Margulès[6], and Paola Caselli[1]
[1] Center for Astrochemical Studies, Max-Planck-Institut für extraterrestrische Physik, Gießenbachstr. 1, D-85748 Garching bei München Germany
bizzocchi@mpe.mpg.de
[2] Dipartimento di Chimica "G. Ciamician," Università di Bologna, via F. Selmi 2, I-40126 Bologna, Italy; mattia.melosso2@unibo.it
[3] Dipartimento di Chimica Industriale "Toso Montanari," Università di Bologna, viale del Risorgimento 4, I-40136 Bologna Italy
[4] Université Paris-Saclay, Institut des Sciences Moléculaires d'Orsay, F-91405 Orsay, France
[5] SOLEIL Synchrotron, AILES beamline, l'Orme des Merisiers, Saint-Aubin, F-91190 Gif-sur-Yvette, France
[6] Université Lille, CNRS, UMR8523—PhLAM—Physique des Lasers Atomes et Molécules, F-59000 Lille, France
Received 2019 November 8; revised 2020 February 3; accepted 2020 February 3; published 2020 April 1

Abstract

Observations of ammonia in interstellar environments have revealed high levels of deuteration, and all its D-containing variants, including ND_3, have been detected in cold prestellar cores and around young protostars. The observation of these deuterated isotopologues is very useful for elucidating the chemical and physical processes taking place during the very early stages of star formation, as the abundance of deuterated molecules is highly enhanced in dense and cold gas. Nitrogen hydride radicals are key species lying at the very beginning of the reaction pathway leading to the formation of NH_3 and organic molecules of prebiotic interest, but relatively little is known about their D-bearing isotopologues. To date, only ND has been detected in interstellar gas. To aid the identification of further deuterated nitrogen radicals, we have thoroughly reinvestigated the rotational spectrum of NHD by employing two different instruments: a frequency-modulation submillimeter spectrometer operating in the THz region and a synchrotron-based Fourier-transform infrared spectrometer operating in the 50–240 cm^{-1} frequency range. NHD was produced in a plasma of NH_3 and D_2. A wide range of rotational energy levels have been probed thanks to the observation of high-N (up to 15) and high-K_a (up to 9) transitions. A global analysis including our new data and data from the literature has provided a comprehensive set of very accurate spectroscopic parameters. A highly reliable line catalog has been generated to assist archival data searches and future astronomical observations of NHD at submillimeter and THz regimes.

Unified Astronomy Thesaurus concepts: Laboratory astrophysics (2004); High resolution spectroscopy (2096); Line positions (2085); Spectral line lists (2082); Interstellar medium (847); Interstellar molecules (849); Isotopic abundances (867)

Supporting material: tar.gz file

1. Introduction

Nitrogen is among the most abundant elements in the universe and is a constituent of essentially all molecules that are important for life as we know it. Nitrogen-bearing species are also ubiquitous in the interstellar medium (ISM) and circumstellar envelopes where about 60 such molecules have been detected to date (McGuire 2018; see also http://astrochymist.org/ and CDMS,[7] Endres et al. 2016). The main molecular reservoir of nitrogen in the ISM is believed to be the homonuclear form N_2. Observation of this molecule, however, is extremely challenging for the following reasons: (1) a lack of a permanent dipole moment, due to its centrosymmetric nature, prevents this species from having a rotational signature; (2) its vibrational mode is infrared inactive. Consequently, a single interstellar detection of N_2 through its electronic spectrum in the far-ultraviolet has been reported to date (Knauth et al. 2004). The study of nitrogen chemistry in space thus mainly relies on observations of other molecules.

Light nitrogen hydrides such as as imidogen (NH), amidogen (NH_2), and ammonia (NH_3) are involved in the very first steps of the reaction network that leads to the formation of complex species, and are thus of primary importance for constraining models describing nitrogen chemistry in the ISM. They are formed by a chain of hydrogen abstraction reactions starting from

$$N^+ + H_2 \longrightarrow NH^+ + H, \quad (1)$$

which eventually produce the ions NH_2^+, NH_3^+, and NH_4^+, which themselves are connected to the corresponding neutral hydrides by dissociative recombination reactions (Dislaire et al. 2012; Le Gal et al. 2014).

The ion–neutral process (1) is endothermic and is thus very sensitive to the H_2 ortho-to-para ratio in the cold ($T < 20$ K) and dense ISM. Also, if H_2 is replaced with its singly deuterated form HD, the endothermicity of (1) is reduced (see, e.g., Cernicharo et al. 2013), thus favoring, in principle, the formation of ND^+ and further D-substituted species (the so called "fractionation"). However, given that the HD/H_2 ratio keeps constants to $\sim 10^{-5}$ (Linsky 2007), this route is rather inefficient, and it is likely that reactions of neutral species with H_2D^+, which abound in the dense and cold environment, could be efficient drivers of D-fractionation (e.g., Sipilä et al. 2019). This process is triggered by favorable thermochemistry (deuterated isotopologues typically have lower zero-point energy than their corresponding parent species), and if suitable

[7] Cologne Database for Molecular Spectroscopy, https://cdms.astro.uni-koeln.de/classic/.

chemical conditions are met (i.e., freeze-out of CO onto dust grains Caselli et al. 1999, 2002), it can be very effective in enhancing the abundances of D-bearing species in cold and dense environments.

Albeit statistically improbable owing to the relatively low cosmic elemental abundance of deuterium ($D/H \sim 1.6 \times 10^{-5}$), multiply deuterated variants of ammonia are known to be present in space (see, e.g., Roueff et al. 2005), including the triply substituted ND_3 (Lis et al. 2002; van der Tak et al. 2002), whose estimated abundance ($ND_3/NH_3 \sim 10^{-3}$–10^{-4}) implies an isotopic enhancement of up to 12 orders of magnitude (Ceccarelli et al. 2007).

Interestingly enough, among the ammonia progenitors, only ND has been detected in space so far (Bacmann et al. 2010, 2016) even though significant abundances of NHD and ND_2 are predicted by chemical models (Roueff et al. 2005). This lack of detection can be attributed to the elusiveness of nitrogen hydride radicals. Indeed, being light molecules, their rotational spectral features are located in the submillimeter to far-infrared (FIR) ranges, where Earth-based observations face the limitation of high atmospheric opacity. This spectral window has been widely opened in the last decade by the *Herschel Space Telescope* campaign (Pilbratt et al. 2010), thus triggering increased interest in the spectroscopic properties of light molecules, hydrides in particular. Nowadays, with ALMA at its full capabilities, wide portions of the submillimeter regime, up to ~1 THz, have become more accessible from the ground, and further insights can be foreseen with the improvement of the SOFIA airborne observatory (see, e.g., Yorke et al. 2018), in particular with the upcoming commissioning of the 4GREAT receiver, which is designed to replicate most of the spectral coverage of the *Herschel*/HIFI instrument. Still, high-frequency observations remain a challenging task and a successful detection of the spectral features of light molecular tracers critically depends on the accuracy of the corresponding rest frequencies.

From a spectroscopic point of view, the parent species NH_2 has been widely studied in the laboratory over the past 40 yr (Davies et al. 1976; Charo et al. 1981; Hills & Cook 1982; Tonooka et al. 1997; Müller et al. 1999; Gendriesch et al. 2001; Martin-Drumel et al. 2014), while much less extensive data sets are available for the other amidogen isotopologues. Driven by the perspectives of current observational facilities, the symmetric species $^{15}NH_2$ and ND_2 species have been recently reinvestigated at high resolution in the millimeter and FIR domains (Margulès et al. 2016; Melosso et al. 2017), and the rotational spectrum of the fully substituted $^{15}ND_2$ variant has been reported for the first time (Melosso et al. 2019). A thorough spectroscopic study is still missing for the asymmetric singly substituted NHD species, which is likely to be the most abundant deuterated variant of amidogen in the ISM. In the early 1980s, the hyperfine structure of a few lines of NHD were observed using the Microwave-Optical Double Resonance technique (Brown & Steimle 1980; Steimle et al. 1980), whereas the first extensive investigation of its rotational spectrum was accomplished much later by Morino & Kawaguchi (1997), who employed a Fourier-transform (FT) FIR spectrometer. Almost simultaneously, Kobayashi et al. (1997) published an analogous study in the millimeter/submillimeter domain using a microwave absorption spectrometer. In the former case, the spectral resolution did not allow observation of the hyperfine structure, but the spectral coverage (103–363 cm^{-1}) led to a detailed centrifugal distortion analysis. In the latter case, hyperfine splittings were resolved for many transitions, and several spin–spin and spin–rotation constants were determined for ^{14}N, H, and D.

In this work, we report: (i) the extension toward the THz regime of the rotational spectrum of NHD with high measurement accuracy, i.e., better than 100 kHz, and (ii) a reinvestigation of its FIR spectrum, recorded at higher resolution (0.001 cm^{-1}) using synchrotron radiation at the AILES beamline of the SOLEIL synchrotron. Newly observed and previously recorded data were analyzed together in order to produce a unique set of highly accurate spectroscopic constants. The structure of the paper is as follows: in Section 2, we describe the laboratory measurements; in Section 3, we provide an account of the data used in the analysis and give a brief description of the Hamiltonian employed to compute the rotational, fine-structure, and hyperfine energies. We discuss the results in Section 4, and draw our conclusions in Section 5.

2. Experiments

High-resolution pure rotational spectral data of NHD have been collected in the submillimeter region at the Centre for Astrochemical Studies of the Max-Planck-Institut für extraterrestrische Physik in Garching (CAS@MPE) and in the FIR domain at the AILES beamline of the SOLEIL synchrotron in Gif-sur-Yvette.

The measurements in Garching were carried out using the CASAC (CAS Absorption Cell) spectrometer associated with a discharge absorption cell for studies of reactive species (Bizzocchi et al. 2018). A detailed description of the instrument has been given previously (Bizzocchi et al. 2017); we report here only a few key details that apply to the present investigation. Several solid-state multiplier/amplifier chains (Virginia Diodes), driven by a radiofrequency synthesizer, have been used as radiation sources. Below 1.1 THz we have employed the WR9.0SGX module, working in the 80–125 GHz interval, associated with a series of active and passive harmonic doublers/triplers in cascade, thus achieving frequency-multiplication factors as high as 9. Measurements above 1.1 THz have been performed with a standalone active multiplier system operating in the 1.1–1.2 THz (AMC-680) interval. Accurate frequency and phase stabilization are achieved by locking the parent centimeter synthesizer to an Rb atomic clock. A closed-cycle He-cooled InSb hot electron bolometer operating at 4 K (QMC) is used as a detector. The measurements have been performed using the frequency modulation (FM) technique to improve the signal-to-noise ratio (S/N). In each frequency range, the FM depth was chosen to approximately match the Doppler half-width of the absorption signals, i.e., 500 kHz at 0.5 THz, and 1300 kHz at 1.2 THz. The carrier signal is modulated by a 33.3 kHz sine wave and the detector output is demodulated at twice this frequency using a phase-sensitive amplifier (2*f* detection). In this way, the second derivative of the actual absorption profile is recorded by the computer-controlled acquisition system. An additional S/N improvement is achieved by filtering the signal into an *RC* circuit.

The NHD radical was produced in a glow discharge (70 mA, ~1.1 kV) of a 1:2 mixture of NH_3 (4 μbar) and D_2 (8 μbar) diluted in Ar buffer gas (total pressure ~25 μbar), with the cell kept at ~180 K by cold vapor/liquid N_2 circulation. In addition to preventing the cell from overheating, the cooling was found

to be critical to improving the amidogen production in the plasma. At temperatures below 180 K, NHD signals decreased due to massive ammonia condensation on the cold cell walls. The spectrum was recorded in selected frequency regions from 430 GHz to 1.2 THz. Slow (0.67–1.67 MHz s^{-1}) back-and-forth scans around target lines were performed with a frequency step of 10–25 kHz and a time constant $RC = 3$ ms.

The FIR spectrum of NHD has been recorded at the synchrotron facility SOLEIL using a Bruker IFS125HR FTIR spectrometer exploiting the bright synchrotron radiation extracted by the AILES beamline. The spectrum results from the coaddition of 104 scans recorded at the ultimate resolution of the instrument, $R = 0.001\ cm^{-1}$ in terms of Bruker definition, in the 50–250 cm^{-1} range. A 6 μm Mylar beamsplitter and a 4.2 K liquid helium-cooled bolometer were used. The NHD radical was produced using a post-discharge setup successfully employed in the past to produce the NH_2 and NH radicals as well as their ^{15}N isotopic variants (Bailleux et al. 2012; Martin-Drumel et al. 2014; Margulès et al. 2016). In this configuration, a radiofrequency discharge cell is connected perpendicularly to the center of a White-type multipass absorption cell. In the present work, a 2.5 m baselength White-type cell allowing 150 m of absorption path length was used (Pirali et al. 2012). The absorption cell was separated from the interferometer by two polypropylene films of 60 μm thickness. The spectrometer was pumped down to 10^{-4} mbar by means of a turbomolecular pump, while the flow in the post-discharge experiment was ensured by a booster pump. The NHD radical was produced by a 1000 W radio-frequency discharge (Martin-Drumel et al. 2011) in a $ND_3 + H_2$ mixture at partial pressures of 30 and 15 μbar, respectively. Production of NHD, as well as ND_2, were found to be more efficient when the gas mixture was injected at one end of the absorption cell while pumping connections were set at the other end of that cell, such that no gas was directly injected through the RF discharge cell. This configuration enabled a propagation of the plasma into the absorption cell. A discharge-off reference spectrum was also recorded to quickly identify the lines arising from transient species.

3. Observed Spectra and Analysis

Monodeuterated amidogen is an asymmetric-top rotor belonging to the C_s point group symmetry. Because of the presence of one unpaired electron in a a'' non-bonding orbital, NHD is a radical with a $\tilde{X}^2A''$ electronic ground state. The electric dipole moment lies in the *ab* principal symmetry plane with components $\mu_a = 0.67$ D and $\mu_b = 1.69$ D (Brown et al. 1979). The rotational spectrum of NHD is very complex due to the coupling of the molecular rotation with various electronic and nuclear spin angular momenta. The electron spin ($S = 1/2$) couples with the rotational angular momentum and splits each rotational level with $N > 0$ into two fine-structure sublevels having $J = N + 1/2$ and $J = N - 1/2$ quantum numbers. Each of these sublevels is further split by hyperfine interactions due to the nuclear spins of ^{14}N ($I = 1$), H ($I = 1/2$), and D ($I = 1$). The chosen angular momentum coupling scheme can be summarized as:

$$\boldsymbol{J} = \boldsymbol{N} + \boldsymbol{S}, \tag{2a}$$

$$\boldsymbol{F}_1 = \boldsymbol{J} + \boldsymbol{I}_N, \tag{2b}$$

$$\boldsymbol{F}_2 = \boldsymbol{F}_1 + \boldsymbol{I}_H, \tag{2c}$$

$$\boldsymbol{F} = \boldsymbol{F}_2 + \boldsymbol{I}_D, \tag{2d}$$

where $\boldsymbol{N}$ and $\boldsymbol{S}$ are the rotational and electron spin angular momenta, whereas $\boldsymbol{I}_X$ (X = N, D, H) represents the various nuclear spin angular momenta. In Equation (2), the nuclear spins are ordered according to the approximate magnitude of their hyperfine coupling.

The effective Hamiltonian can be expressed as a sum of several energy contributions as in the following (Kobayashi et al. 1997; Morino & Kawaguchi 1997):

$$\tilde{H}_{\rm eff} = \tilde{H}_{\rm rot} + \tilde{H}_{\rm sr} + \tilde{H}_{\rm hfs}. \tag{3}$$

Here, $\tilde{H}_{\rm rot}$ is the Watson A-reduced Hamiltonian in its I^r representation (Watson 1977), which includes the rotational energy and the centrifugal distortion (up to the J^{12} terms in the present analysis). The fine-structure Hamiltonian $\tilde{H}_{\rm sr}$ contains the electron spin–rotation terms (ϵ tensor) and their centrifugal dependencies. The $\tilde{H}_{\rm hfs}$ term is the hyperfine-structure Hamiltonian that includes electronic spin–nuclear spin interactions (a_F, $\boldsymbol{T}$) and nuclear spin–nuclear spin coupling ($\boldsymbol{C}$) for all three nuclei, and the electric quadrupole coupling contributions (χ) for the ^{14}N and D nuclei, having $I \geqslant 1$. The spectral computation was performed using the SPFIT/SPCAT suite of programs (Pickett 1991) which implements all the matrix elements of the Hamiltonian (3) in the coupling scheme (2).

Unlike the symmetric species NH_2 and ND_2, for which a π rotation around the b principal axis exchanges two identical particles, there are no spin statistics in the case of NHD. Consequently, all fine and hyperfine sublevels, up to a maximum of 36, are allowed for each N_{K_a,K_c} rotational level. The electric dipole selection rules (Gordy & Cook 1984) on this sublevel manifold produce very complex hyperfine patterns for each rotational transition due to the additional fine/hyperfine selection rules $\Delta J = 0, \pm 1$, $\Delta F_1 = 0, \pm 1$, $\Delta F_2 = 0, \pm 1$, and $\Delta F = 0, \pm 1$. The most intense components have $\Delta J = \Delta F_1 = \Delta F_2 = \Delta F = \Delta N$. An example of the complexity is given in Figure 1, which illustrates the above described interactions for the fundamental b-type transition $N_{K_a,K_c} = 1_{11} - 0_{00}$. Each line of the fine-structure doublet, separated by some GHz, is then split in a multitude of hyperfine components, roughly gathered in loose triplets, due to the dominant effect of electron spin–nuclear spin coupling due to the ^{14}N nucleus.

3.1. Submillimeter Spectrum

The spectral recordings performed with the CASAC spectrometer covered the frequency interval from 430 to 1200 GHz, exploring the region above 520 GHz for the first time. Since NHD is a very light molecule, the rotational transitions are quite isolated in the spectrum and separated by several tens of GHz. The transitions recorded in this frequency domain are summarized in Table 1, which also reports the hypothetically unsplit frequency of the rotational lines and the number of assigned hyperfine components.

Under our experimental conditions, isolated NHD absorption lines have an FWHM of 1.5–3.0 MHz due to the sizable Doppler-broadening characteristic of this spectral range (e.g., $\Delta\nu_G^{\rm FWHM} \sim$ 1.5 MHz at 700 GHz for NHD at 150 K). However, due to the complexity of the hyperfine structure, overlap of numerous components is common and blends of lines, resolved to different extents, are typically observed. To facilitate the retrieval of the

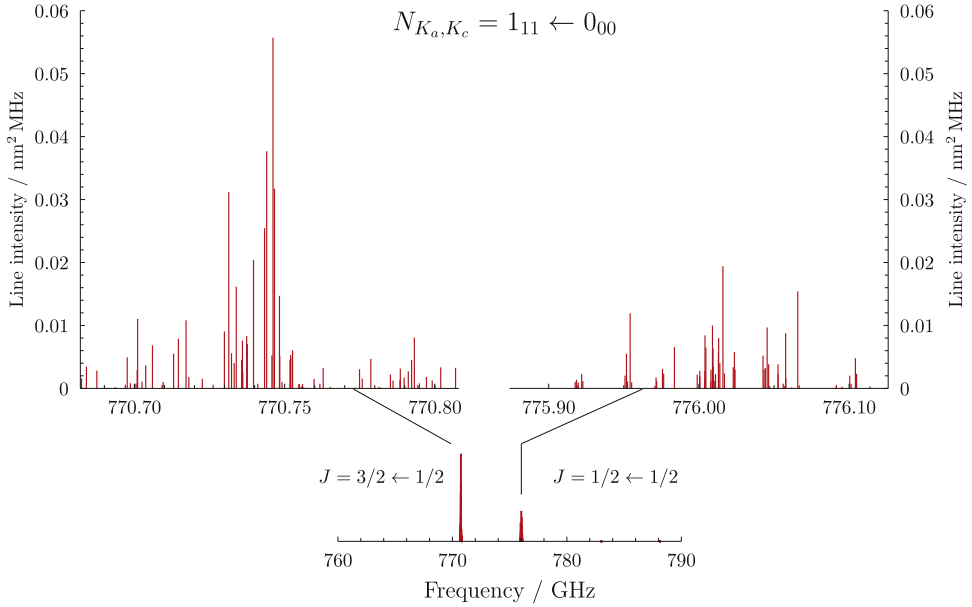

Figure 1. Stick spectrum of the $N_{Ka,Kc} = 1_{1,1} - 0_{0,0}$ rotational transition of NHD simulated at 298 K.

Table 1
List of NHD Rotational Transitions with HFS Recorded in the Submillimeter Region

Line	Type[a]	Unsplit Freq. (MHz)	No. of FS Lines	No. of HFS Lines
$1_{1,0} - 1_{0,1}$	${}^{b}Q_{+1,-1}$	432580.3	4	44
$2_{0,2} - 1_{1,1}$	${}^{b}R_{-1,+1}$	456235.5	2	5
$2_{1,1} - 2_{0,2}$	${}^{b}Q_{+1,-1}$	515448.6	2	19
$3_{1,2} - 3_{0,3}$	${}^{b}Q_{+1,-1}$	656654.9	2	30
$1_{1,1} - 0_{0,0}$	${}^{b}R_{+1,+1}$	772506.7	2	15
$4_{1,3} - 4_{0,4}$	${}^{b}Q_{+1,-1}$	869336.3	2	7
$3_{0,3} - 2_{1,2}$	${}^{b}R_{-1,+1}$	902924.7	2	12
$3_{2,1} - 3_{1,2}$	${}^{b}Q_{+1,-1}$	1020828.9	2	5
$6_{2,4} - 6_{1,5}$	${}^{b}Q_{+1,-1}$	1062344.6	2	6
$2_{1,2} - 1_{0,1}$	${}^{b}R_{+1,+1}$	1112159.2	2	4
$3_{1,3} - 2_{1,2}$	${}^{a}R_{0,+1}$	1122794.6	1	1
$5_{1,4} - 5_{0,5}$	${}^{b}Q_{+1,-1}$	1157071.0	1	6
$3_{0,3} - 2_{0,2}$	${}^{a}R_{0,+1}$	1199330.9	2	6

Note.
[a] The symbol ${}^{x}M_{\delta K_a,\delta K_c}$ is used to label in a compact form the transition type for an asymmetric rotor: x indicates the dipole moment component involved; M = P, Q, R is the symbol for the transitions with $\Delta N = -1, 0, +1$, respectively; and δK_a and δK_c refer to the (signed) change in the K_a and K_c pseudoangular quantum numbers (Gordy & Cook 1984).

corresponding central-line frequencies, we have modeled the recorded absorption profiles using the `proFFiT` line-analysis code (Dore 2003), adopting a FM Voigt profile function and considering the full complex representation of the Fourier-transformed dipole correlation function. When necessary, the background contribution has also been accounted for using a third-order polynomial expansion. In most cases, this approach typically allowed for a satisfactory fit of the recorded spectral profiles, with some minor discrepancies due to the occasional presence of noise features or weak interfering lines. An example is presented in Figure 2, which shows the recordings of the $N_{K_a,K_c} = 4_{1,3} \leftarrow 4_{0,4}$, $J = 9/2 \leftarrow 9/2$ fine-structure component of NHD: 18 hyperfine components are blended in 6 resolvable lines illustrating the predominance of the N coupling ($I_N = 1$, three main groups), followed by the H coupling ($I_H = 1/2$, closely separated doublets). The modeled profile has been obtained by fixing the Doppler FWHM at 1.834 MHz (computed at 150 K) and adjusting the line positions and the Lorentzian FWHM (collisional broadening), $\Delta\nu_G^{FWHM} = 1.42(15)$ MHz, assumed equal for all the components.

The described procedure allowed us to obtain line positions with an associate error in the 30–100 kHz interval, depending on the S/N of the spectrum and on the overall goodness of the line-profile fit.

Whenever possible, a single hyperfine transition has been assigned to a given resolved feature detected in the rotational spectrum. Measurements corresponding to tight line blends have been instead assigned to the subset of components that sum up to make the dominant intensity contribution. In these cases the intensity-averaged frequency is compared with the experimental one in the least-squares fit. Loose blends of unresolved components, resulting in very broad or distorted line profiles, have not been used in the analysis.

3.2. Far-infrared Spectrum

The recorded FIR spectrum was calibrated using residual water lines whose accurate frequencies have been reported in the literature (Matsushima et al. 1995); the resulting accuracy for the line frequency is estimated to be 0.0002 cm^{-1}. Deuterium scrambling in the ND_3+H_2 discharge mixture appears very efficient as strong transitions of NHD are observed. About 10 of the strongest lines are saturated and have been excluded from the analysis. As a point of comparison, under the same experimental conditions, in pure ND_3 or NH_3, similarly strong signals of ND_2 and NH_2, respectively, are observed, while in the present spectrum only relatively weak signals of ND_2 (10% absolute absorption at best) and no NH_2 are observed.

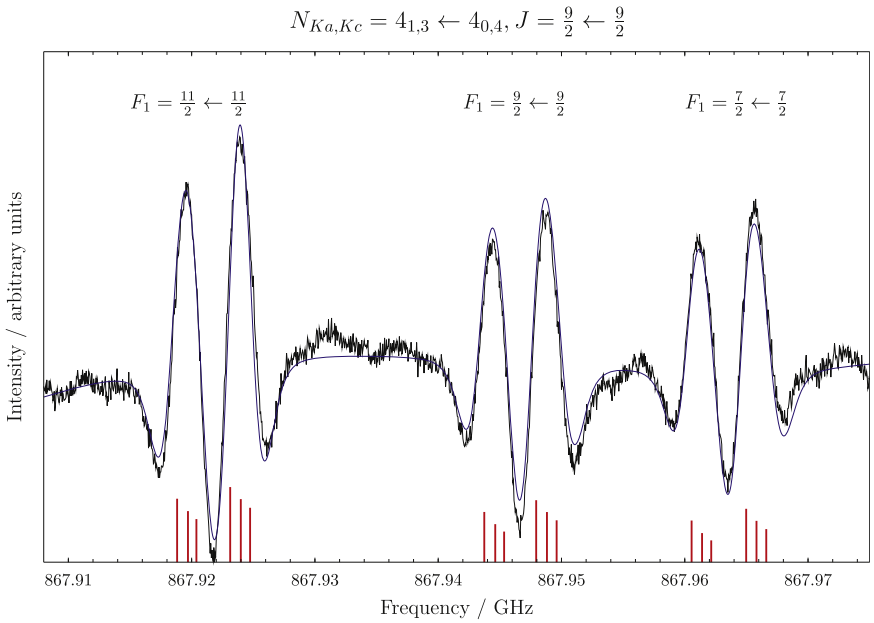

Figure 2. Recording (black trace) of the $N_{K_a,K_c} = 4_{1,3} \leftarrow 4_{0,4}$, $J = 9/2 \leftarrow 9/2$ fine-structure transitions showing six resolvable components. Integration time: 390 s; $RC = 3$ ms; scanning rate: 1.3 MHz s^{-1}; modulation depth: 850 kHz. The blue trace plots the modeled spectrum computed with `proFFiT` using a modulated Voigt profile (see the text). The red sticks indicate the position and relative intensity of the 18 hyperfine components. Note that the F_2 and F quantum numbers are not shown in the plot.

As previously observed in similar studies of the NH_2 radical and its ^{15}N isotopologues (Martin-Drumel et al. 2014; Margulès et al. 2016), the hyperfine splitting due to the nitrogen atom is partially or fully resolved for several *b*-type transitions on the FIR spectrum, as illustrated in Figure 3. Because the natural width of the transitions is smaller than the experimental resolution in this spectral region, many lines exhibit a cardinal sine profile at their base (arising from the boxcar apodization). While this effect can be canceled by applying an apodization to the interferogram before Fourier transform, the resulting width broadening prevented the resolution of the nitrogen hyperfine structure on most transitions; consequently such apodization was not applied.

In total, 512 transitions have been assigned to 447 experimental frequencies in the range 54–236 cm^{-1}, 141 *a*-type, and 371 *b*-type transitions with $N'_{max} = 15$ (for $K'_a = 0 - 2$) and $K'_{a\,max} = 7$ (for $N' = 7$). Among these transitions, 107 transitions (80 different frequencies, mostly *b*-type) with $K'_a = 0 - 3$ exhibit partially or fully resolved nitrogen hyperfine structure. The uncertainty on line frequency is doubled for lines that appear broadened by unresolved hyperfine structure or asymmetric splitting.

4. Results

The experimental frequencies were fitted to the Hamiltonian of Equation (3) in a least-squares procedure, in which the weight of each datum was proportional to the inverse square of its error. The data set includes previously measured (Kobayashi et al. 1997; Morino & Kawaguchi 1997) and newly observed millimeter-wave, submillimeter-wave, and FIR transitions. The data from Morino & Kawaguchi (1997) were given uncertainties of 7.5×10^{-4} cm^{-1}, i.e., an order of magnitude smaller than their resolution of 0.0075 cm^{-1}, while the errors reported in Kobayashi et al. (1997) were retained. A total of 58 spectroscopic parameters could be determined from the analysis of more than 1000 distinct frequencies. Their values are reported in Table 2 and 3 and compared with the results of former studies.

All the observed transition frequencies could be fitted within their experimental uncertainty: the weighted deviation of the fit is close to one ($\sigma = 0.96$) and the rms error is 52 kHz for transitions in the millimeter/submillimeter-wave region and 4.1×10^{-4} cm^{-1} for those in the FIR (1.9×10^{-4} cm^{-1}, for the transitions recorded in this work). While the studies of Morino & Kawaguchi (1997) and Kobayashi et al. (1997), published almost simultaneously, provided two different sets of constants from different data sets, our combined analysis comprises all those transitions, in addition to a larger set of submillimeter-wave and FIR data. In this respect, a more comprehensive set of spectroscopic constants is produced in this work. Overall, the rotational, centrifugal distortion, and fine-interaction constants of Table 2 are now refined, and their values agree well with those reported previously by the cited authors. Still, some sporadic discrepancies are present, e.g., the Φ_{NK} constant determined by Kobayashi et al. (1997) is two times larger than ours and has the opposite sign. The hyperfine-interaction parameters are almost identical to those of Kobayashi et al. (1997), because the magnitude of the hyperfine coupling effect decreases with increasing the rotational quantum numbers involved in the transitions. We have determined 23 hyperfine constants, 3 more than in Kobayashi et al. (1997), namely: $\chi_{bb} - \chi_{cc}$ for the nucleus D, $\Delta^J T_{aa}$, and C_{cc} for the nucleus H. The magnitude of these parameters is small and they are determined with a precision of 30% at best. Still, their inclusion in the fit allowed the reduction of σ by 10%, thus they have been retained in the final analysis.

While the semi-rigid rotor Hamiltonian used in this work allows us to nicely reproduce the experimental data at experimental accuracy, owing to the use of high order centrifugal distortion terms, it is possible, however, that the present analysis has reached its limit. Indeed, seven additional

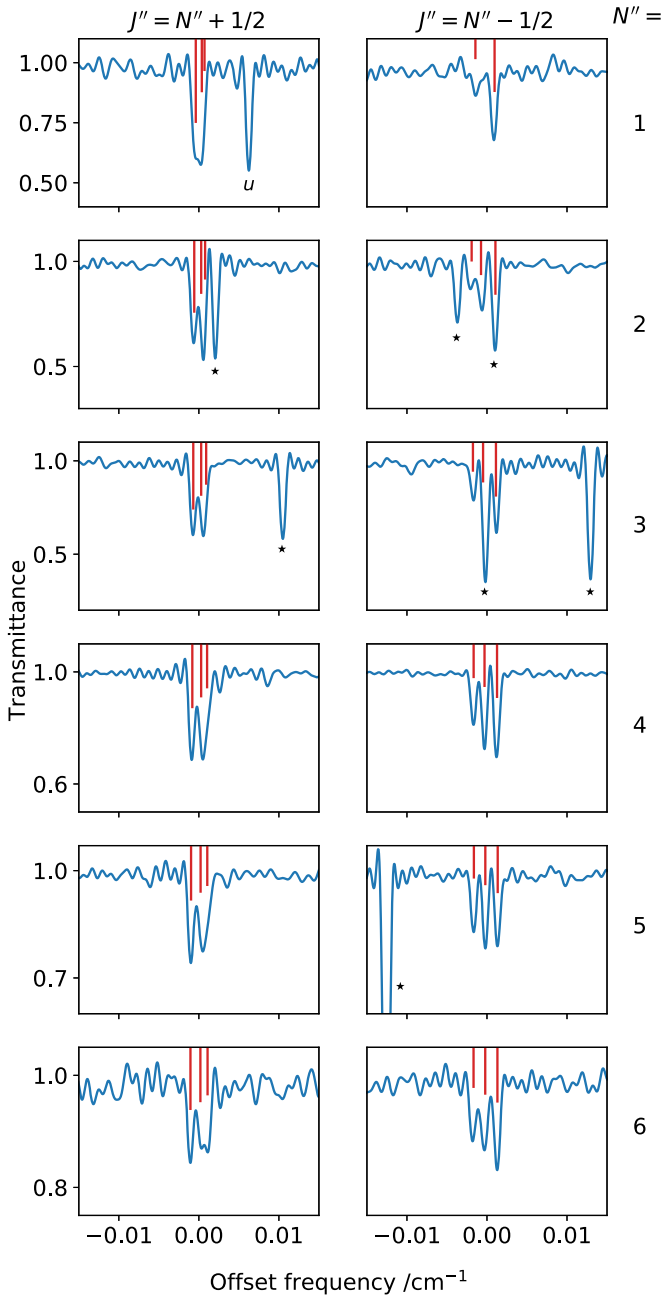

Figure 3. Observation on the FIR spectrum of the hyperfine structure due to the nuclear spin of the N atom in NHD for the *b*-type $^rR(1)$ branch with $K_a'' + K_c'' - N'' = 0$. Frequencies are reported as the offset frequencies from the predicted transition when no hyperfine structure is taken into account and span the 68–188 cm^{-1} range (see the two .dat files in the .tar.gz package for the numerical values). The predicted frequency of each component (neglecting the H and D hyperfine splittings) is indicated by the red sticks (intensity in arbitrary units). Transitions labeled with "⋆" symbol are still present with the discharge off and most likely arise from ND_3; the line labeled with a "*u*" remains unassigned.

transitions involving high $N + K_a$ values have been assigned with relative confidence on the FIR spectrum but could not be reproduced in the fit. As for NH_2 (Martin-Drumel et al. 2014), a dedicated model taking into account the anomalous centrifugal distortion of this very light radical may be better suited to reproducing these data. Considering the small number of transitions involved, however, no attempt was made in this direction in the present study and these transitions are reported in the datafile.txt file in the .tar.gz package.

Table 2
Rotational and Fine-structure Spectroscopic Parameters Determined for NHD

Constants		Present Work	Kobayashi et al. (1997)	Morino & Kawaguchi (1997)
A	/MHz	602874.1082(64)	602873.269(18)	602879.3(24)
B	/MHz	243153.818(15)	243150.415(29)	243147.6(9)
C	/MHz	169872.513(15)	169875.877(26)	169871.5(9)
Centrifugal distortion				
Δ_N	/MHz	9.29361(23)	9.2833(9)	9.239(9)
Δ_{NK}	/MHz	31.2187(11)	30.303(13)	31.226(45)
Δ_K	/MHz	250.2294(21)	250.825(10)	250.90(21)
δ_N	/MHz	3.07038(10)	3.04088(12)	3.0672(30)
δ_K	/MHz	48.7864(81)	46.854(14)	47.502(66)
Φ_N	/kHz	1.0098(24)		0.785(42)
Φ_{NK}	/MHz	0.04883(14)	−0.0901(11)	0.04569(60)
Φ_{KN}	/MHz	−0.17115(50)		−0.1638(21)
Φ_K	/MHz	0.79326(48)	0.59213(25)	0.8223(87)
ϕ_N	/kHz	0.4888(12)		0.475(18)
ϕ_{NK}	/MHz	0.023248(49)		0.02099(42)
ϕ_K	/MHz	0.2588(11)		0.1256(19)
L_{NNK}	/kHz	−2.373(14)		
L_{KKN}	/kHz	0.0437(32)		0.0615(84)
L_K	/kHz	−3.91(29)		−3.20(17)
l_K	/kHz	0.307(22)		0.0210(48)
P_K	/Hz	8.43(29)		17.6(16)
p_K	/Hz	−1.40(16)		
O_K	/Hz	−0.0196(18)		−0.0591(57)
Fine interaction				
ϵ_{aa}	/MHz	−7043.123(16)	−7043.180(27)	−7041.0(12)
ϵ_{bb}	/MHz	−1149.383(17)	−1149.38(9)	−1150.96(45)
ϵ_{cc}	/MHz	7.809(17)	7.82(8)	8.7(11)
$(\epsilon_{ab} + \epsilon_{ba})/2$	/MHz	1088.64(60)	1093.9(11)	1056(7)
Δ_N^S	/MHz	0.12026(78)	0.1187(20)	0.140(9)
Δ_{KN+NK}^S	/MHz	0.2401(87)		
Δ_{NK}^S	/MHz	1.77(35)	0.234(13)	
Δ_K^S	/MHz	16.2441(91)	16.245(12)	16.16(21)
δ_N^S	/MHz	0.06300(30)	0.0640(7)	0.075(8)
δ_K^S	/MHz	0.9553(83)	0.96(4)	1.20(11)
Φ_K^S	/MHz	−0.06755(59)	−0.0634(7)	−0.0570(45)
L_K^S	/kHz	0.2270(96)		0.135(30)
Number of FIR lines		649		
Number of MW lines		353		
rms_{FIR}	/cm^{-1}	4.2×10^{-4}		
rms_{MW}	/kHz	51.8		
σ		0.963		
N'_{max} , $K'_{a,max}$		15,9		

Note. Numbers in parenthesis are one standard deviation in units of the last quoted digit.

5. Conclusions

The rotational spectrum of NHD has thoroughly been reinvestigated from the submillimeter region to the FIR. A frequency-modulation spectrometer and a synchrotron-based FT spectrometer were used to perform the measurements. Numerous *a*-type and *b*-type transitions have been recorded with high accuracy, i.e., 30–100 kHz for lines up to 1.2 THz and 2×10^{-4} cm^{-1} in the 50–240 cm^{-1} frequency range. Also, the astronomically important $N_{Ka,Kc} = 1_{1,1} - 0_{0,0}$ fundamental *b*-type transition has been observed in the laboratory for the first time and its fine and hyperfine components have been accurately measured around 770 GHz ($J = 3/2 - 1/2$) and 776 GHz ($J = 1/2 - 1/2$).

Table 3
Hyperfine Spectroscopic Parameters (MHz) Determined for NHD

Constant	Atom	This Work	Kobayashi et al. (1997)
a_F	(N)	28.1077(71)	28.124(10)
$\Delta^K a_F$	(N)	0.0	−0.0157(12)
T_{aa}	(N)	−43.3319(77)	−43.329(8)
T_{bb}	(N)	−44.2125(97)	−44.218(11)
T_{ab}	(N)	0.550	0.550
χ_{aa}	(N)	−0.288(13)	−0.297(14)
$(\chi_{bb} - \chi_{cc})$	(N)	−6.738(28)	−6.725(32)
χ_{ab}	(N)	1.370	1.370
C_{aa}	(N)	0.3486(33)	0.3505(37)
C_{bb}	(N)	0.0738(29)	0.0742(37)
χ_{aa}	(D)	0.167(15)	0.143(40)
$(\chi_{bb} - \chi_{cc})$	(D)	0.100(44)	…
a_F	(D)	−10.230(10)	−10.229(13)
T_{aa}	(D)	8.0530(91)	8.052(10)
T_{bb}	(D)	−7.251(13)	−7.251(14)
T_{ab}	(D)	6.1(14)	6.7(14)
C_{aa}	(D)	0.0482(34)	0.0491(36)
a_F	(H)	−67.128(11)	−67.116(13)
T_{aa}	(H)	−23.305(31)	−23.254(24)
T_{bb}	(H)	28.460(23)	28.434(22)
T_{ab}	(H)	−47.9(19)	−48.7(20)
$\Delta^K T_{aa}$	(H)	−0.122(16)	−0.0621(51)
$\Delta^J T_{aa}$	(H)	0.0192(69)	…
C_{aa}	(H)	0.0844(75)	0.1152(64)
C_{bb}	(H)	0.0864(50)	0.1042(60)
C_{cc}	(H)	−0.0157(48)	…

Note. Numbers in parentheses are one standard deviation in units of the last quoted digit. Parameters without a reported deviation were kept fixed in the fit.

The newly obtained set of spectroscopic parameters (Tables 2 and 3) allow us to generate a very reliable set of rest frequencies for NHD in the submillimeter and FIR spectral domains. Considering all rotational transitions originating from levels at energy E/h lower than 300 K, their corresponding rest frequencies have a 1σ uncertainty of less than $10\,\mathrm{m\,s^{-1}}$ (in radial equivalent velocity) up to 3 THz. Two different CDMS-like catalogs based on the present spectral calculations, with hyperfine structure fully resolved or ^{14}N coupling only, are provided in the .cat files in the .tar.gz package. This comprehensive laboratory study has implications for the first identification of NHD in space, which would be a step toward a more complete understanding of ammonia formation in the ISM. Indeed, the highly precise rest frequencies provided here enable one to carry out focused searches in the observation data of the Herschel Legacy Archive (http://archives.esac.esa.int/hsa/whsa/) and also provide a basis for new observations in the presently accessible spectral windows employing facilities like ALMA or the upcoming 4GREAT instrument on board SOFIA.

This study was supported by Bologna University (RFO funds) and by MIUR (Project PRIN 2015: STARS in the CAOS, grant No. 2015F59J3R). The work at SOLEIL has been performed under the proposal 20110017 and was supported by the Programme National "Physique et Chimie du Milieu Interstellaire" (PCMI) of CNRS/INSU with INC/INP cofunded by CEA and CNES.

Appendix
Supplementary Material

The catalog `nhd_full_hfs.cat` lists all the hyperfine components originated by ^{14}N, D, and H nuclear couplings and extends up to 2 THz (150 μm). The catalog `nhd_n_hfs.cat` contains a computation of the hyperfine spectrum due to the ^{14}N coupling only and extends into the FIR domain (8 THz ∼38 μm). The file `center_frequencies.dat` reports the reference frequencies used in Figure 3. The file `discarded_transitions.dat` contains those transitions which could not be reproduced in the fit and were excluded from the analysis. The machine-readable table `measured_transitions.mrt` lists all measured transition frequencies and fit residuals. All the files are available in the .tar.gz package.

ORCID iDs

Luca Bizzocchi https://orcid.org/0000-0002-9953-8593
Luca Dore https://orcid.org/0000-0002-1009-7286
Filippo Tamassia https://orcid.org/0000-0003-4145-7827
Marie-Aline Martin-Drumel https://orcid.org/0000-0002-5460-4294
Paola Caselli https://orcid.org/0000-0003-1481-7911

References

Bacmann, A., Caux, E., Hily-Blant, P., et al. 2010, A&A, 521, L42
Bacmann, A., Daniel, F., Caselli, P., et al. 2016, A&A, 587, 26
Bailleux, S., Martin-Drumel, M. A., Margulès, L., et al. 2012, A&A, 538, A135
Bizzocchi, L., Lattanzi, V., Laas, J., et al. 2017, A&A, 602, A34
Bizzocchi, L., Melosso, M., Dore, L., et al. 2018, ApJL, 863, 3
Brown, J. M., Chalkley, S. W., & Wayne, F. D. 1979, MolPh, 38, 1521
Brown, J. M., & Steimle, T. C. 1980, ApJL, 236, 101
Caselli, P., Walmsley, C. M., Tafalla, M., Dore, L., & Myers, P. C. 1999, ApJL, 523, L165
Caselli, P., Walmsley, C. M., Zucconi, A., et al. 2002, ApJ, 565, 344
Ceccarelli, C., Caselli, P., Herbst, E., Tielens, A. G. G. M., & Caux, E. 2007, in Protostars and Planets V, ed. B. Reipurth, D. Jewitt, & K. Keil (Tucson, AZ: Univ. Arizona Press), 47
Cernicharo, J., Tercero, B., Fuente, A., et al. 2013, ApJL, 771, L10
Charo, A., Herbst, E., De Lucia, F. C., & Sastry, K. V. L. N. 1981, ApJL, 244, 111
Davies, P. B., Russell, D. K., Thrush, B. A., & Radford, H. E. 1976, CPL, 42, 35
Dislaire, V., Hily-Blant, P., Faure, A., et al. 2012, A&A, 537, A20
Dore, L. 2003, JMoSp, 221, 93
Endres, C. P., Schlemmer, S., Schilke, P., Stutzki, J., & Müller, H. S. P. 2016, JMoSp, 327, 95
Gendriesch, R., Lewen, F., Winnewisser, G., & Müller, H. S. P. 2001, J. Mol. Struct., 599, 293
Gordy, W., & Cook, R. L. 1984, Microwave Molecular Spectra (New York: Wiley)
Hills, G. W., & Cook, J. M. 1982, JMoSp, 94, 456
Knauth, D. C., Andersson, B. G., McCandliss, S. R., & Warren Moos, H. 2004, Natur, 429, 636
Kobayashi, K., Ozeki, H., Saito, S., Tonooka, M., & Yamamoto, S. 1997, JChPh, 107, 9289
Le Gal, R., Hily-Blant, P., Faure, A., et al. 2014, A&A, 562, A83
Linsky, J. L. 2007, SSRv, 130, 367
Lis, D. C., Roueff, E., Gerin, M., et al. 2002, ApJL, 571, L55
Margulès, L., Martin-Drumel, M. A., Pirali, O., et al. 2016, A&A, 591, A110
Martin-Drumel, M. A., Pirali, O., Balcon, D., et al. 2011, RSciI, 82, 113106
Martin-Drumel, M. A., Pirali, O., & Vervloet, M. 2014, JPCA, 118, 1331
Matsushima, F., Odashima, H., Iwasaki, T., Tsunekawa, S., & Takagi, K. 1995, JMoSt, 352, 371
McGuire, B. A. 2018, ApJS, 239, 17
Melosso, M., Conversazioni, B., Degli Esposti, C., et al. 2019, JQSRT, 222, 186
Melosso, M., Degli Esposti, C., & Dore, L. 2017, ApJS, 233, 15

Morino, I., & Kawaguchi, K. 1997, JMoSp, 182, 428
Müller, H. S. P., Klein, H., Belov, S. P., et al. 1999, JMoSp, 195, 177
Pickett, H. M. 1991, JMoSp, 148, 371
Pilbratt, G. L., Riedinger, J. R., Passvogel, T., et al. 2010, A&A, 518, L1
Pirali, O., Boudon, V., Oomens, J., & Vervloet, M. 2012, JChPh, 136, 024310
Roueff, E., Lis, D. C., van der Tak, F. F. S., Gerin, M., & Goldsmith, P. F. 2005, A&A, 438, 585
Sipilä, O., Caselli, P., & Harju, J. 2019, A&A, 631, A63
Steimle, T. C., Curl, R. F., Jr., & Brown, J. M. 1980, JChPh, 73, 2552
Tonooka, M., Yamamoto, S., Kobayashi, K., & Saito, S. 1997, JChPh, 106, 2563
van der Tak, F. F. S., Schilke, P., Müller, H. S. P., et al. 2002, A&A, 388, L53
Watson, J. K. G. 1977, in Vibrational Spectra and Structure, Vol. 6 ed. J. Durig (Amsterdam: Elsevier), 1
Yorke, H. W., Young, E. T., & Becklin, E. E. 2018, Proc. SPIE, 10700, 107000E